
This is an electronic reprint of the original article.
This reprint may differ from the original in pagination and typographic detail.

Conley, Kevin M.; Cocchi, Caterina; Ala-Nissila, Tapio
Formation of Near-IR Excitons in Low-Dimensional CuSbS₂

Published in:
Journal of Physical Chemistry C

DOI:
[10.1021/acs.jpcc.1c06530](https://doi.org/10.1021/acs.jpcc.1c06530)

Published: 30/09/2021

Document Version
Publisher's PDF, also known as Version of record

Published under the following license:
CC BY

Please cite the original version:
Conley, K. M., Cocchi, C., & Ala-Nissila, T. (2021). Formation of Near-IR Excitons in Low-Dimensional CuSbS₂. *Journal of Physical Chemistry C*, 125(38), 21087–21092. <https://doi.org/10.1021/acs.jpcc.1c06530>

This material is protected by copyright and other intellectual property rights, and duplication or sale of all or part of any of the repository collections is not permitted, except that material may be duplicated by you for your research use or educational purposes in electronic or print form. You must obtain permission for any other use. Electronic or print copies may not be offered, whether for sale or otherwise to anyone who is not an authorised user.

Formation of Near-IR Excitons in Low-Dimensional CuSbS₂

Kevin M. Conley, Caterina Cocchi, and Tapio Ala-Nissila*

Cite This: *J. Phys. Chem. C* 2021, 125, 21087–21092

Read Online

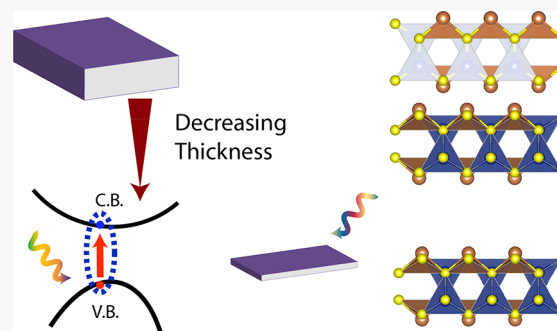
ACCESS |

Metrics & More

Article Recommendations

Supporting Information

ABSTRACT: The electronic and optical properties of low-dimensional semiconductors are typically quite different from those of their bulk counterparts. Yet, the optical gap of two-dimensional copper antimony disulfide (CuSbS₂) does not dramatically change with decreasing thickness of the material. The absorption onset remains at about 1.5 eV in the monolayer, bilayer, and bulk materials. Using density functional theory and many-body perturbation theory, we rationalize this behavior through the interplay of quantum confinement, electron–hole interactions, and the formation of surface states. Specifically, the spatial confinement in thin layers induces strongly bound optical transitions in the near-infrared region. Our results explain the optical properties in copper antimony disulfide platelets of varying thickness and set these materials as potential candidates for novel photovoltaic devices and near-infrared sensors.



INTRODUCTION

Thin-film materials for solar photovoltaics are challenging traditional wafer silicon in the renewable energy sector.^{1–5} Scarcity and competing industrial demands for the constituent elements of CdTe and copper indium gallium disulfide/diselenide devices have driven the search for alternative systems with comparable performance.^{5–7} Among them, CuSbS₂ is a promising material formed by earth-abundant elements and characterized by a large absorption coefficient at relevant frequencies for solar light harvesting.^{8,9} The optical gap of bulk CuSbS₂ ranges between 1.3 and 1.5 eV.^{7,10–13} Theoretical studies based on quantum density functional theory (DFT) calculations^{14,15} have shown that in this material the fundamental gap is indirect, like in bulk silicon, and that the direct gap appears at a marginally higher energy of 1.73 eV.^{16–20}

Recently, single-crystal CuSbS₂ platelets of varying thickness have been experimentally prepared using the hot injection method.^{21,22} This bottom-up approach enables the synthesis of nanomaterials with well-defined size and homogeneous shape down to monolayer thickness.²² Interestingly, in CuSbS₂, quantum confinement effects accompanying the nanostructuring process do not lead to a sizable increase of the optical gap, as typically observed in low-dimensional semiconductors and insulators in comparison with their bulk counterparts.^{23–27} For example, in transition metal dichalcogenides, spatial confinement increases absorption and photoluminescence^{28–34} or even induces superconductivity.³⁵ Enhancement of optical activities has also been observed in hexagonal boron nitride^{36–38} and heterostructures thereof,^{39,40} as well as in the more recently produced silicene.^{41–44}

Such peculiar behavior of CuSbS₂ has already been explored in a DFT study,⁴⁵ which, however, has not been able to convincingly rationalize the change of the optical gap of thin platelets (1–5 nm) of this material compared to the bulk. Understanding the fundamental mechanism that is responsible for this counterintuitive behavior is essential to fully exploit the potential of CuSbS₂ in optoelectronic and photovoltaic applications. Most importantly, it is mandatory to gain further insight into exotic behaviors of quantum-confined semiconductors.

In this work, based on DFT and many-body perturbation theory (MBPT),⁴⁶ we rationalize why the optical gap of two-dimensional CuSbS₂ platelets does not increase compared to their bulk counterparts. From the analysis of the band structure, the density of states, the charge-density distribution, and finally the dielectric and optical response of this material in the monolayer, bilayer, and bulk form, we ascribe this behavior to the concurrent contribution of localized surface states that are formed in the nanoconfined systems and strongly bound excitons that appear therein.

METHODS

All calculations presented in this work are performed with the Vienna *ab initio* simulation package (VASP)⁴⁷ utilizing the projector-augmented wave (PAW) method.^{48,49} The electronic

Received: August 10, 2021

Published: September 20, 2021



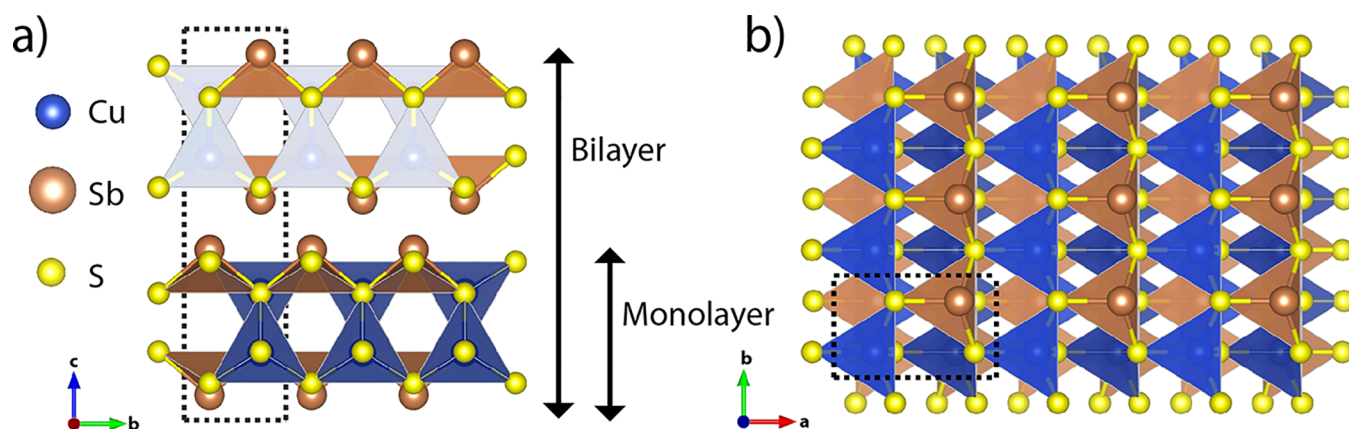


Figure 1. (a) Layered and (b) bulk CuSbS_2 with Cu, Sb, and S atoms shown as blue, brown, and yellow spheres.

structure was calculated using DFT with the Heyd–Scuseria–Ernzerhof (HSE06) hybrid functional.⁵⁰ A $4 \times 6 \times 2$ k -point mesh and 370 eV cutoff are used, and the structures were assumed to be relaxed when the forces on each atom were smaller than $10 \text{ meV } \text{\AA}^{-1}$. The mono- and bilayer structures are simulated including in the unit cell 9 \AA of vacuum along the (001) surface in order to prevent unphysical interactions between the replicas. We checked this value by ensuring the band gap remained constant with an additional vacuum and by checking that the total charge density decays to less than $1 \times 10^{-6} a_0^{-3}$ in the nonperiodic direction.

The quasiparticle band structures are calculated with a single-shot G_0W_0 approach applied on top of the HSE06 electronic structure. The GW band structure converged with 600 bands or 320 bands in the case of the monolayer. The optical properties were calculated by solving the Bethe–Salpeter equation (BSE)⁵¹ and included contributions beyond the Tamm–Dancoff approximation.⁵² The 30 highest valence and the 60 lowest conduction bands are considered in the bilayer and bulk, and the 28 highest valence and the 60 lowest conduction bands are considered in the monolayer. Spurious contributions arising from the vacuum in the layered structures are excluded by rescaling the dielectric permittivity with the effective volume of the layer.

RESULTS AND DISCUSSION

The optimized lattice constants and atomic positions obtained for bulk CuSbS_2 (Figure 1) are consistent with previous findings in the literature obtained on similar footing^{16,17} (see Table S1 in the Supporting Information). CuSbS_2 is an orthorhombic crystal with space group $Pnma$. The space groups of the bilayer and monolayer are $P2_1/m$ and Pm , respectively. In the layered crystals, no surface reconstruction is found, although the atoms are bound closer together normal to the (001) surface. Specifically, the material volume in the monolayer shrinks by 4.2% compared to the bulk, as an effect of the quantum confinement along the c axis (see Figure 1a), in agreement with experimental findings on powder CuSbS_2 platelets.²² In the bilayer, this reduction is only 0.8%.

From the analysis of the electronic properties, we find for bulk CuSbS_2 an indirect fundamental gap of 1.67 eV, as predicted from DFT using HSE06 (see Figure 2a), in agreement with previous calculations.^{16,17,45} Despite quantum confinement, both monolayer and bilayer CuSbS_2 exhibit smaller band gaps than the bulk, with the former featuring the narrowest gap. The inclusion of the quasi-particle correction

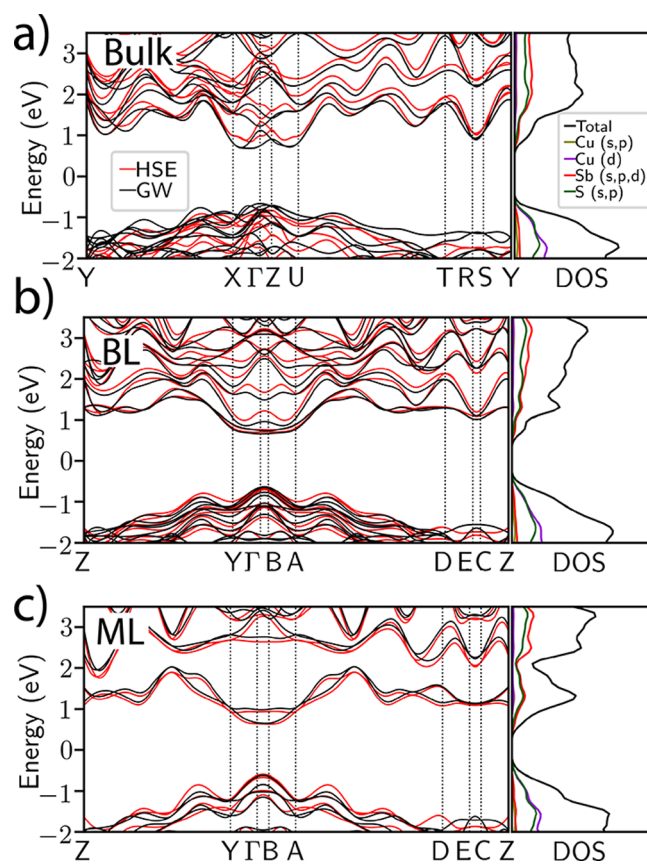


Figure 2. GW (black lines) and HSE06 band structure (red lines) of (a) bulk, (b) bilayer (BL), and (c) monolayer (ML) CuSbS_2 . The density of states and atom-projected contributions calculated using HSE06 are shown adjacent to the band structures.

via the perturbative G_0W_0 approach applied on top of the HSE06 electronic structure leads to a reduction of the band gap in both the bulk and bilayer and to an increase in the monolayer. The nature of the gap (indirect in the bulk and direct in the low-dimensional sheets) is unaffected by the inclusion of the self-energy contribution (see Table 1).

The crossover from indirect- to direct-band-gap material going from bulk to the mono- and bilayer is ubiquitous in layered semiconductors.^{28,33,53,54} In order to understand this behavior in CuSbS_2 , we analyze the band dispersion shown in Figure 2. The Brillouin zone of each system is shown in Figure

Table 1. Band Gaps and Optical Transitions of Bulk and Layered CuSbS₂

	indirect band gap (eV)	direct band gap (eV)	E_{optical} (eV)	E_{b} (eV)
Bulk				
this work, MBPT	1.35	1.40	1.20	0.20
this work, HSE06	1.67	1.71		
HSE06 ¹⁶	1.68	1.73		
HSE06 ¹⁷	1.69			
Layered				
this work, MBPT BL		1.30	0.95	0.35
this work, MBPT ML		1.30	0.76	0.54
this work, HSE06 BL		1.38		
this work, HSE06 ML		1.25		
Experimental				
platelets (25–50 nm thick) ²²	1.51 ^a	1.57 ^a	0.92 ^b	0.65 ^c
platelets (1–5 nm thick) ²²	1.44 ^a	1.52 ^a	1.04 ^b	0.48 ^c

^aOptical gap measured using diffuse reflectance spectroscopy.

^bEnergies less than 0.85 eV were beyond the experimental range.

^cThe experimental binding energy, E_{b} , was obtained by subtracting the optical transition energy from the direct optical gap.

S1. In the bulk material, the valence band maximum of bulk CuSbS₂ lies between the Γ and Z points, and the conduction band minimum lies between the Γ and X points. The smallest, direct gap lies between the Γ and X points. Interestingly, in the layered materials, the highest valence band and the lowest conduction bands flatten along the B and Y directions. This change in the band dispersion is responsible for the crossover to a direct band gap. The variation in the fundamental band gap in increasingly confined layers is attributed to the reduced band dispersion accompanied by the formation of a surface state at the Sb-terminated (001) surface. The states have Cu d and S sp character at the top of the valence band and S sp and Sb spd character at the bottom of the conduction band (Figure 2). There is no significant change in the character of the states in the layered materials. The partial DOS of bulk CuSbS₂ is consistent with previous DFT studies in bulk CuSbS₂.²⁰

To confirm the presence of surface states in the Sb-terminated dangling surface of mono- and bilayer CuSbS₂, we inspect the electron density at the conduction band minimum. The results plotted along a two-dimensional slice in the (001)

plane (see Figure 3) confirm that the electron density accumulates at the surface of the low-dimensional structures. The electron density between the layers in the bilayer is similar to the interlayer electron density in the bulk material. The electron density spills out of the monolayer more than the bilayer (Figure 3c). This results in electron density accumulation between the adjacent surface Sb atoms.

Having clarified the electronic characteristics of low-dimensional CuSbS₂, we complete our analysis by inspecting its optical properties, calculated by solving the BSE⁵¹ of MBPT. Bright excitations below the fundamental band gap occur at 1.20, 0.95, and 0.76 eV for the bulk material, bilayer, and monolayer, respectively, as a signature of excitonic effects (see Figure 4 as well as Figure S2 for the real part and the out-

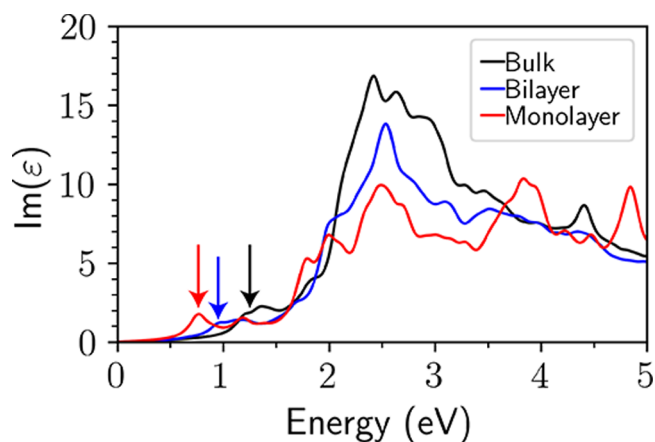


Figure 4. Imaginary component of the dielectric permittivity of bulk, bilayer, and monolayer CuSbS₂ in the in-plane directions calculated using GW+BSE. The lowest-energy optical transition in each structure is marked with an arrow.

of-plane components). The contributions of the BSE eigenstates to each exciton are represented as a fat band plot in reciprocal space (Figure S3). The contributions between the direct electron–hole pairs are predominately from the bands near the band gap. The strength of the contributions is more in the layered materials, which have a reduced band dispersion. The exciton binding energy, calculated as $E_{\text{b}} = E_{\text{g}}^{\text{GW}} - E_{\text{optical}}$, is 0.20 eV in the bulk where E_{g}^{GW} is the direct gap from GW and E_{optical} is the lowest-energy excitation from BSE. The reduced

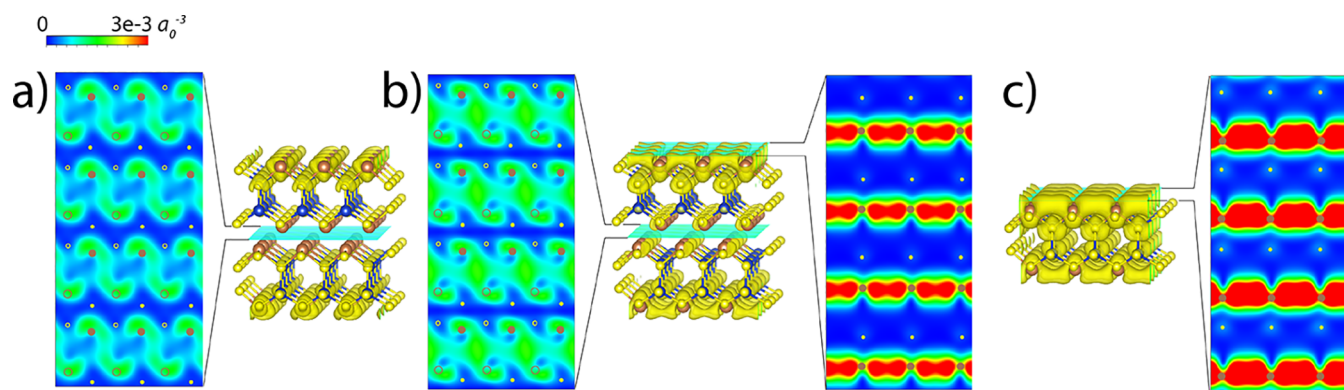


Figure 3. Spatial distribution of the probability density associated with the conduction band minimum of (a) bulk, (b) bilayer, and (c) monolayer CuSbS₂ calculated from DFT. The displayed isosurface value is $0.003 a_0^{-3}$. The positions of atoms above (below) the considered plane are marked by open (closed) circles: brown for Sb and yellow for S.

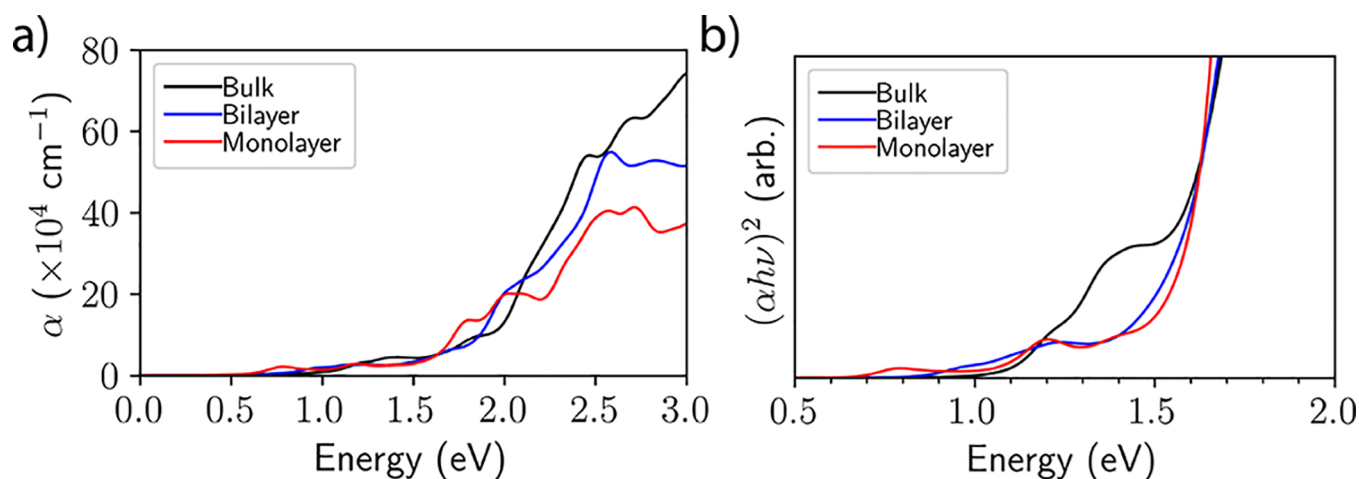


Figure 5. (a) Absorption coefficient, α , and (b) Tauc plot for bulk, bilayer, and monolayer CuSbS_2 in the in-plane direction calculated using GW+BSE.

dimensionality of the system increases the exciton binding energy to 0.35 eV in the bilayer and to 0.54 eV in the monolayer (see Table 1). The experimental binding energy is similar to the prediction from theory despite the natural size distribution of platelets in the powder samples.²² Furthermore, the effects of ligand passivation, defects, or stacking of monolayers into towers could obscure the band gap crossover and optical properties.⁵⁵ Experimental detection of the changes in the excitonic peaks or lattice would be improved if the ensemble contains only monolayer platelets. We also note that the possible exciton-like peaks in the layered material may be resolved at lower temperatures, which was previously shown for bulk CuSbS_2 .⁵⁶

For a closer comparison with experimental results, it is convenient to display the optical properties of each material in the form of the absorption coefficient and Tauc plot. The absorption coefficient is $\alpha = 4\pi\kappa/\lambda$, where κ is the extinction coefficient and λ the wavelength of the incident light. From the plot in Figure 5a, we notice that the absorption coefficient increases above 10^5 cm^{-1} between 1.7 and 1.9 eV regardless of dimensionality. In particular, the Tauc plot in Figure 5b shows that (i) despite the spatial confinement in the low-dimensional structures the absorption increases steeply at about 1.5 eV in the bulk, bilayer, and monolayer and (ii) weak optical excitations appear below the band gap in all materials, as anticipated in the discussion of the dielectric permittivity (Figure 4). The first finding, (i), is consistent with recent results from diffuse reflectance spectroscopy on platelets which detected only a small decrease (0.05 eV) in the direct optical gap energy in thin (1 to 5 nm) platelets compared to the thickest platelets (25–50 nm).²² The second finding, (ii), is supported by the presence of weak absorption peaks below the optical gap that have been detected in the ellipsometric data of bulk CuSbS_2 ⁵⁶ and two-dimensional platelets.²² The thinnest platelets had a peak at 1.04 eV, and energies less than 0.85 eV were beyond the spectral range.²²

CONCLUSIONS

In summary, by means of DFT and many-body calculations, we rationalized the peculiar behavior of CuSbS_2 which exhibits a reduction of the lowest optical transition going from the bulk to mono- and bilayer films. In addition to the crossover from indirect- to direct-band-gap materials, bilayer and monolayer

films of CuSbS_2 exhibit (slightly) reduced band gaps compared to their bulk counterpart due to the formation of localized surface states on the dangling facet. On top of this, now in agreement with physical intuition, larger exciton binding energies were found upon increasing quantum confinement, which led to the decrease of the absorption onset going to the bulk, bilayer, and monolayer, with the latter absorbing radiation in the near-infrared region. By disclosing the fundamental mechanisms behind the peculiar electronic and optical properties of CuSbS_2 , this study opens important perspectives for nanoengineering this material and related compounds for optoelectronic and photovoltaic applications.

ASSOCIATED CONTENT

Supporting Information

The Supporting Information is available free of charge at <https://pubs.acs.org/doi/10.1021/acs.jpcc.1c06530>.

Relaxed lattice constants and out-of-plane dielectric permittivities for each structure (PDF)

AUTHOR INFORMATION

Corresponding Author

Tapio Ala-Nissila – QTF Centre of Excellence, Department of Applied Physics, Aalto University School of Science, FI-00076 Aalto, Finland; Interdisciplinary Centre for Mathematical Modelling, Department of Mathematical Sciences, Loughborough University, Loughborough, Leicestershire LE11 3TU, United Kingdom; Email: tapio.ala-nissila@aalto.fi

Authors

Kevin M. Conley – Department of Chemistry and Materials Science, Aalto University School of Chemical Engineering, FI-00076 Aalto, Finland; orcid.org/0000-0001-7780-3096

Caterina Cocchi – Institut für Physik, Carl von Ossietzky Universität Oldenburg, 26129 Oldenburg, Germany; Institut für Physik und IRIS Adlershof, Humboldt-Universität zu Berlin, 12489 Berlin, Germany

Complete contact information is available at: <https://pubs.acs.org/doi/10.1021/acs.jpcc.1c06530>

Notes

The authors declare no competing financial interest.

ACKNOWLEDGMENTS

This work was performed as part of the Academy of Finland RADDESS project 314488 and QTF Centre of Excellence program (project 312298) (KC, TAN). We acknowledge computational resources provided by the CSC – IT Center for Science (Finland) and by the Aalto Science-IT project (Aalto University School of Science). The work was supported in part by the High Performance Computing Centre Stuttgart (HLRS) and HPC-Europa3. C.C. acknowledges financial support from the German Research Foundation, project number 182087777 (CRC 951), from the German Federal Ministry of Education and Research (Professorinnenprogramm III), and from the State of Lower Saxony (Professorinnen für Niedersachsen).

REFERENCES

- (1) Walsh, A.; Chen, S.; Wei, S.-H.; Gong, X.-G. Kesterite thin-film solar cells: Advances in materials modelling of $\text{Cu}_2\text{ZnSnS}_4$. *Adv. Energy Mater.* **2012**, *2*, 400–409.
- (2) Mitzi, D. B.; Gunawan, O.; Todorov, T. K.; Barkhouse, D. A. R. Prospects and performance limitations for Cu–Zn–Sn–S–Se photovoltaic technology. *Philos. Trans. R. Soc., A* **2013**, *371*, 20110432.
- (3) Pal, K.; Singh, P.; Bhaduri, A.; Thapa, K. B. Current challenges and future prospects for a highly efficient (> 20%) kesterite CZTS solar cell: A review. *Sol. Energy Mater. Sol. Cells* **2019**, *196*, 138–156.
- (4) Ramanujam, J.; Bishop, D. M.; Todorov, T. K.; Gunawan, O.; Rath, J.; Nekovei, R.; Artegiani, E.; Romeo, A. Flexible CIGS, CdTe and a-Si: H based thin film solar cells: A review. *Prog. Mater. Sci.* **2020**, *110*, 100619.
- (5) Peter, L. M. Towards sustainable photovoltaics: The search for new materials. *Philos. Trans. R. Soc., A* **2011**, *369*, 1840–1856.
- (6) Fthenakis, V.; Wang, W.; Kim, H. C. Life cycle inventory analysis of the production of metals used in photovoltaics. *Renewable Sustainable Energy Rev.* **2009**, *13*, 493–517.
- (7) Peccerillo, E.; Durose, K. Copper–antimony and copper–bismuth chalcogenides—Research opportunities and review for solar photovoltaics. *MRS Energy & Sustainability* **2018**, *5*, No. E13.
- (8) Kumar, M.; Persson, C. Cu (Sb, Bi)(S, Se)₂ as indium-free absorber material with high optical efficiency. *Energy Procedia* **2014**, *44*, 176–183.
- (9) de Souza Lucas, F. W.; Peng, H.; Johnston, S.; Dippe, P. C.; Lany, S.; Mascaro, L. H.; Zakutayev, A. Characterization of defects in copper antimony disulfide. *J. Mater. Chem. A* **2017**, *5*, 21986–21993.
- (10) Rodriguez-Lazcano, Y.; Nair, M.; Nair, P. CuSbS_2 thin film formed through annealing chemically deposited Sb_2S_3 – CuS thin films. *J. Cryst. Growth* **2001**, *223*, 399–406.
- (11) Kyono, A.; Kimata, M. Crystal structures of chalcostibite (CuSbS_2) and emplectite (CuBiS_2): Structural relationship of stereochemical activity between chalcostibite and emplectite. *Am. Mineral.* **2005**, *90*, 162–165.
- (12) Zhou, J.; Bian, G.-Q.; Zhu, Q.-Y.; Zhang, Y.; Li, C.-Y.; Dai, J. Solvothermal crystal growth of CuSbQ_2 (Q = S, Se) and the correlation between macroscopic morphology and microscopic structure. *J. Solid State Chem.* **2009**, *182*, 259–264.
- (13) Ikeda, S.; Kawaguchi, T.; Koda, Y.; Iiyama, N.; Harada, T.; Nakanishi, S.; Nakatsuka, S.; Nose, Y. Structural and electric properties of CuSbS_2 compound semiconductor bulk crystals. *Jpn. J. Appl. Phys.* **2018**, *57*, 08RC09.
- (14) Hohenberg, P.; Kohn, W. Inhomogeneous Electron Gas. *Phys. Rev.* **1964**, *136*, B864–B871.
- (15) Kohn, W.; Sham, L. J. Self-Consistent Equations Including Exchange and Correlation Effects. *Phys. Rev.* **1965**, *140*, A1133–A1138.
- (16) Temple, D. J.; Kehoe, A. B.; Allen, J. P.; Watson, G. W.; Scanlon, D. O. Geometry, electronic structure, and bonding in CuMCh_2 (M = Sb, Bi; Ch = S, Se): Alternative solar cell absorber materials? *J. Phys. Chem. C* **2012**, *116*, 7334–7340.
- (17) Dufton, J. T.; Walsh, A.; Panchmatia, P. M.; Peter, L. M.; Colombara, D.; Islam, M. S. Structural and electronic properties of CuSbS_2 and CuBiS_2 : Potential absorber materials for thin-film solar cells. *Phys. Chem. Chem. Phys.* **2012**, *14*, 7229–7233.
- (18) Birkett, M. Optical properties of earth-abundant semiconductors for renewable energy. *Ph.D. thesis*, University of Liverpool, 2016.
- (19) Gassoumi, A.; Musa Saad, M. H.-E.; Alfaify, S.; Ben Nasr, T.; Bouarissa, N. The investigation of crystal structure, elastic and optoelectronic properties of CuSbS_2 and CuBiS_2 compounds for photovoltaic applications. *J. Alloys Compd.* **2017**, *725*, 181–189.
- (20) Gupta, G. K.; Chaurasiya, R.; Dixit, A. Thermodynamic stability and optoelectronic properties of Cu (Sb/Bi)(S/Se)₂ ternary chalcogenides: Promising ultrathin photoabsorber semiconductors. *Sol. Energy* **2019**, *177*, 679–689.
- (21) Moosakhani, S.; Sabbagh Alvani, A. A.; Mohammadpour, R.; Hannula, P.-M.; Ge, Y.; Hannula, S.-P. Platelet CuSbS_2 particles with a suitable conduction band position for solar cell applications. *Mater. Lett.* **2018**, *215*, 157–160.
- (22) Moosakhani, S.; Sabbagh Alvani, A. A.; Mohammadpour, R.; Ge, Y.; Hannula, S.-P. Solution synthesis of CuSbS_2 nanocrystals: A new approach to control shape and size. *J. Alloys Compd.* **2018**, *736*, 190–201.
- (23) Novoselov, K. S.; Geim, A. K.; Morozov, S. V.; Jiang, D.; Zhang, Y.; Dubonos, S. V.; Grigorieva, I. V.; Firsov, A. A. Electric field effect in atomically thin carbon films. *Science* **2004**, *306*, 666–669.
- (24) Butler, S. Z.; Hollen, S. M.; Cao, L.; Cui, Y.; Gupta, J. A.; Gutierrez, H. R.; Heinz, T. F.; Hong, S. S.; Huang, J.; Ismach, A. F.; et al. Progress, challenges, and opportunities in two-dimensional materials beyond graphene. *ACS Nano* **2013**, *7*, 2898–2926.
- (25) Liu, B.; Abbas, A.; Zhou, C. Two-dimensional semiconductors: From materials preparation to electronic applications. *Adv. Electron. Mater.* **2017**, *3*, 1700045.
- (26) Turkowski, V.; Din, N. U.; Rahman, T. S. Time-dependent density-functional theory and excitons in bulk and two-dimensional semiconductors. *Computation* **2017**, *5*, 39.
- (27) Mounet, N.; Gibertini, M.; Schwaller, P.; Campi, D.; Merkys, A.; Marrazzo, A.; Sohier, T.; Castelli, I. E.; Cepellotti, A.; Pizzi, G.; et al. Two-dimensional materials from high-throughput computational exfoliation of experimentally known compounds. *Nat. Nanotechnol.* **2018**, *13*, 246–252.
- (28) Mak, K. F.; Lee, C.; Hone, J.; Shan, J.; Heinz, T. F. Atomically thin MoS_2 : A new direct-gap semiconductor. *Phys. Rev. Lett.* **2010**, *105*, 136805.
- (29) Jariwala, D.; Sangwan, V. K.; Lauhon, L. J.; Marks, T. J.; Hersam, M. C. Emerging device applications for semiconducting two-dimensional transition metal dichalcogenides. *ACS Nano* **2014**, *8*, 1102–1120.
- (30) Voshell, A.; Terrones, M.; Rana, M. In *Wide bandgap power and energy devices and applications III*; Matin, M., Chowdhury, S., Dutta, A. K., Eds.; SPIE, 2018; Vol. 10754; pp 66 – 83.
- (31) Mueller, T.; Malic, E. Exciton physics and device application of two-dimensional transition metal dichalcogenide semiconductors. *npj 2D Mater. Appl.* **2018**, *2*, 1–12.
- (32) Lau, K. W.; Cocchi, C.; Draxl, C. Electronic and optical excitations of two-dimensional ZrS_2 and HfS_2 and their heterostructure. *Phys. Rev. Mater.* **2019**, *3*, 074001.
- (33) Edalati-Boostan, S.; Cocchi, C.; Draxl, C. MoTe_2 as a natural hyperbolic material across the visible and the ultraviolet region. *Phys. Rev. Mater.* **2020**, *4*, 085202.
- (34) Liang, Q.; Zhang, Q.; Zhao, X.; Liu, M.; Wee, A. T. Defect engineering of two-dimensional transition-metal dichalcogenides: Applications, challenges, and opportunities. *ACS Nano* **2021**, *15*, 2165–2181.
- (35) Choi, W.; Choudhary, N.; Han, G. H.; Park, J.; Akinwande, D.; Lee, Y. H. Recent development of two-dimensional transition metal dichalcogenides and their applications. *Mater. Today* **2017**, *20*, 116–130.

- (36) Cassabois, G.; Valvin, P.; Gil, B. Hexagonal boron nitride is an indirect bandgap semiconductor. *Nat. Photonics* **2016**, *10*, 262–266.
- (37) Paleari, F.; Galvani, T.; Amara, H.; Ducastelle, F.; Molina-Sánchez, A.; Wirtz, L. Excitons in few-layer hexagonal boron nitride: Davydov splitting and surface localization. *2D Mater.* **2018**, *5*, 045017.
- (38) Wickramaratne, D.; Weston, L.; Van de Walle, C. G. Monolayer to bulk properties of hexagonal boron nitride. *J. Phys. Chem. C* **2018**, *122*, 25524–25529.
- (39) Aggoune, W.; Cocchi, C.; Nabok, D.; Rezouali, K.; Akli Belkhir, M.; Draxl, C. Enhanced light–matter interaction in graphene/h-BN van der Waals heterostructures. *J. Phys. Chem. Lett.* **2017**, *8*, 1464–1471.
- (40) Bawari, S.; Pal, S.; Pal, S.; Mondal, J.; Narayanan, T. N. Enhanced photo-electrocatalytic hydrogen generation in graphene/hBN van der Waals structures. *J. Phys. Chem. C* **2019**, *123*, 17249–17254.
- (41) Li, X.; Mullen, J. T.; Jin, Z.; Borysenko, K. M.; Buongiorno Nardelli, M.; Kim, K. W. Intrinsic electrical transport properties of monolayer silicene and MoS₂ from first principles. *Phys. Rev. B: Condens. Matter Mater. Phys.* **2013**, *87*, 115418.
- (42) Li, H.; Hui-Xia, F.; Meng, S. Silicene: From monolayer to multilayer—A concise review. *Chin. Phys. B* **2015**, *24*, 086102.
- (43) Houssa, M.; Dimoulas, A.; Molle, A. Silicene: A review of recent experimental and theoretical investigations. *J. Phys.: Condens. Matter* **2015**, *27*, 253002.
- (44) Chowdhury, S.; Jana, D. A theoretical review on electronic, magnetic and optical properties of silicene. *Rep. Prog. Phys.* **2016**, *79*, 126501.
- (45) Ramasamy, K.; Sims, H.; Butler, W. H.; Gupta, A. Mono-, few-, and multiple layers of copper antimony sulfide (CuSbS₂): A ternary layered sulfide. *J. Am. Chem. Soc.* **2014**, *136*, 1587–1598.
- (46) Onida, G.; Reining, L.; Rubio, A. Electronic excitations: Density-functional versus many-body Green's-function approaches. *Rev. Mod. Phys.* **2002**, *74*, 601–659.
- (47) Kresse, G.; Furthmüller, J. Efficiency of ab-initio total energy calculations for metals and semiconductors using a plane-wave basis set. *Comput. Mater. Sci.* **1996**, *6*, 15–50.
- (48) Blöchl, P. E. Projector augmented-wave method. *Phys. Rev. B: Condens. Matter Mater. Phys.* **1994**, *50*, 17953.
- (49) Kresse, G.; Joubert, D. From ultrasoft pseudopotentials to the projector augmented-wave method. *Phys. Rev. B: Condens. Matter Mater. Phys.* **1999**, *59*, 1758.
- (50) Heyd, J.; Scuseria, G. E.; Ernzerhof, M. Hybrid functionals based on a screened Coulomb potential. *J. Chem. Phys.* **2003**, *118*, 8207–8215.
- (51) Salpeter, E. E.; Bethe, H. A. A relativistic equation for bound-state problems. *Phys. Rev.* **1951**, *84*, 1232.
- (52) Sander, T.; Maggio, E.; Kresse, G. Beyond the Tamm-Dancoff approximation for extended systems using exact diagonalization. *Phys. Rev. B: Condens. Matter Mater. Phys.* **2015**, *92*, 045209.
- (53) Tongay, S.; Zhou, J.; Ataca, C.; Lo, K.; Matthews, T. S.; Li, J.; Grossman, J. C.; Wu, J. Thermally driven crossover from indirect toward direct bandgap in 2D semiconductors: MoSe₂ versus MoS₂. *Nano Lett.* **2012**, *12*, 5576–5580.
- (54) Mudd, G. W.; Molas, M. R.; Chen, X.; Zolyomi, V.; Nogajewski, K.; Kudrynskiy, Z. R.; Kovalyuk, Z. D.; Yusa, G.; Makarovskiy, O.; Eaves, L.; Potemski, M.; Fal'ko, V. I.; Patane, A.; et al. The direct-to-indirect band gap crossover in two-dimensional van der Waals indium selenide crystals. *Sci. Rep.* **2016**, *6*, 1–10.
- (55) Moosakhani, S.; Sabbagh Alvani, A. A.; Mohammadpour, R.; Sainio, J.; Ge, Y.; Hannula, S.-P. Effect of sulfonating agent and ligand chemistry on structural and optical properties of CuSbS₂ particles prepared by heat-up method. *CrystEngComm* **2018**, *20*, 1527–1535.
- (56) Birkett, M.; Savory, C. N.; Rajpalke, M. K.; Linhart, W. M.; Whittles, T. J.; Gibbon, J. T.; Welch, A. W.; Mitrovic, I. Z.; Zakutayev, A.; Scanlon, D. O.; et al. Band gap temperature-dependence and exciton-like state in copper antimony sulphide, CuSbS₂. *APL Mater.* **2018**, *6*, 084904.